RSC Advances

ROYAL SOCIETY OF CHEMISTRY

www.rsc.org/advances

Journal Name

ARTICLE

Facile Synthesis of Mesoporous FeNi-alloyed Carbonaceous Microsphere as Recyclable Magnetic Adsorbent for Trichloroethylene Removal

Xinxin Liu[a], Dong Zhang[b], Biao Guo[a], Yue Qu[a], Ge Tian[a], Huijuan Yue[a]*, Shouhua Feng[a]

Magnetic mesoporous FeNi/CS composites (FeNi alloy embedded in porous carbon sphere) have been synthesized via a facile one-pot hydrothermal carbonization method, using metal nitrates and glucose as magnetic particle precursors and carbon source, respectively. Properties of FeNi/CS were characterized with X-ray diffraction (XRD), Raman spectra, scanning electron microscopy (SEM) system, transmission electron microscopy (TEM), thermo-gravimetric analysis (TGA), nitrogen adsorption/desorption isotherms and magnetic property measurement system (SQUID-VSM). FeNi/CS derived from different pyrolysis temperatures of 500, 700, 900°C (FeNi/CS-500, FeNi/CS-700, FeNi/CS-900, respectively) could serve as the novel magnetic carbonaceous adsorbent for removing trichloroethylene from aqueous media. FeNi/CS produced at 700 °C has the best removal capacity among all, mainly due to its large surface area, a wider range of pore size distribution, and suitable carbonized extent. The pseudo-second order model is well fitted to the kinetic data, indicating that chemisorption is the primary mechanism of TCE adsorption onto FeNi/CS. Moreover, the obtained magnetic porous composites could be easily separated from solution by using a permanent magnet after adsorbing TCE and used as efficient and recyclable adsorbents in the successive removal of TCE from wastewater.

received 00th January 20xx,
Accepted 00th January 20xx

DOI: 10.1039/x0xx00000x

www.rsc.org/

Introduction

Organic pollutants are enemies of environment due to their huge scale of generation from industry, non-washability, slow self-degradation and toxicity.[1,2] Present methodologies to remove pollutants include biological treatment,[3] adsorption,[4-6] chemical oxidation[7] and so on, of which physical adsorption stands out as one of the acceptable remediation techniques due to its simplicity of operation and low cost.[8] Among various kinds of adsorbents, carbon materials are frequently used as effective ones, which are mainly affected by their large surface area, pore size, as well as pore surface chemistry.[9-15] However, a rather complex filtration or centrifugation process is commonly indispensable for phase separation in aqueous system after application, which is one of the main issues in using such conventional carbon materials.[16-19] In order to solve this problem, magnetic separation comes into focus with the virtues of easy isolation and ready regeneration by an applied magnetic field.[20,21] In line with this idea, major attention has been paid to using nano zero-valent iron[17,22-24] iron oxides (Fe_2O_3 and Fe_3O_4)[4,25] and metal ferrites[26] as magnetic carriers to construct magnetic porous carbon adsorbents for removing toxic pollutants.

As important transition metal alloy, the FeNi-alloyed nanoparticles are a class of soft magnetite materials used as catalysis, magnetic resonance imaging (MRI) and electromagnetic absorbing materials, due to their higher saturation magnetization and low coercivity.[27-30] Therefore, with its available chemical stability and magnetic merit, and the advantages of activity of carbon adsorbents, a powerful magnetic carbon material can be formed as a potential

[a] a State Key Laboratory of Inorganic Synthesis and Preparative Chemistry, College of Chemistry, Jilin University, Changchun 130012, P. R. China. Email:huijuan@jlu.edu.cn
[b] b Key Laboratory of Physics and Technology for Advanced Batteries (Ministry of Education), College of Physics, Jilin University, Changchun 130012, P. R. China.
Electronic Supplementary Information (ESI) available: [details of any supplementary information available should be included here]. See DOI: 10.1039/x0xx00000x

adsorbent for water purification. For instance, magnetic FeNi alloy mesoporous carbon nanocomposites for azo dye and tretinoin adsorption were synthesized using mesoporous silica as the template, respectively.[31,32] However, the promising magnetic adsorbents are still limited by multistep synthesis involving a sacrificial inorganic template which is not derived from sustainable resources, which cause the adsorbents too difficult to scale and too expensive for widespread industrial use. Thus, it is still a challenge to develop straightforward approaches to fabricate FeNi alloy endowed mesoporous carbon for improved applications.

Currently, the carbonization of biomass is undoubtedly a facile, low-cost and environment-friendly method to produce porous carbon-coating.[33-35] Herein, we report a series of magnetic composites formed by FeNi alloy nanoparticles embedded in carbon microspheres, using $Fe(NO_3)_3$ and $Ni(NO_3)_2$ as iron and nickel precursors under the reductive environment generated from carbonization of glucose. To the best of our knowledge, the synthesis of mesoporous FeNi-alloyed carbonaceous microsphere by using in-situ glucose carbonization followed by self-reduction remains unexplored yet.

As one of the critical occupational carcinogen stipulated by the United States Environmental Protection Agency (EPA),[36] European Union,[37] and Chinese Center for Disease Control and Prevention,[38] trichloroethylene (TCE) was chosen as a model of organic pollutant for testing the removal activities of the synthesized magnetic carbons in this work. The as-prepared carbon-coated FeNi nanopaticles have been demonstrated to possess great removal capacity of TCE and high removal rate. The batch aqueous TCE remediation kinetics and the effects of carbonization temperature on the properties of the synthesized magnetic carbons were studied. It is noteworthy that the mesoporous FeNi alloy/carbon sphere have good recyclability with a removal efficiency of 75% even after 5th cycle.

Experimental

Materials

Iron(III) nitrate nonahydrate, nickel(II) nitrate hexahydrate, D-glucose and Trichloroethylene were purchased from Sinopharm Chemical Reagent Co. Ltd., China. Alcohol (C_2H_5OH) was purchased from Tianjin Tiantai Fine Chemical Reagent Co. Ltd., China. All the chemicals were used as received without further purification. Deionized water was employed to prepare the solutions in our experiments.

Preparation of mesoporous FeNi alloy/carbon sphere Catalysts

FeNi alloy/carbon sphere were synthesized using in-situ formation from a glucose-induced carbonization and self-reduction. Briefly, 0.36 mmol iron(III) nitrate nonahydrate, 2.5 mmol nickel nitrate hexahydrate together with 7.6 mmol D-glucose were dissolved in 10 ml of ultrapure water, and the mixture was stirred constantly for 4 h at room temperature. The mixed solution was then transferred into a Teflon-lined stainless steel autoclave (16 mL) and stayed in an oven at 180 °C for 22 h. After cooling to room temperature, the black suspension was rinsed with ethanol/water for several times. The precipitate was oven-dried at 80 °C for 5 h. The dried sample was further pyrolyzed in N_2 atmosphere in a tubular furnace at 500, 700, and 900 °C for 2 hours. The obtained products are denoted as FeNi/CS-500, FeNi/CS-700, FeNi/CS-900, respectively.

Carbon sphere was synthesized for comparison by a simple hydrothermal method using glucose as carbon source and pyrolyzed in N_2 atmosphere in a tubular furnace at 700 °C for two hours.

Characterization of Catalysts

The crystalline structure of samples was investigated by a Rigaku D/MAX 2550 V/PC powder X-ray diffraction (XRD). Raman spectra were recorded on a Micro-Raman (Renishaw) system, equipped with an Ar laser (514.5 nm). The patterns were collected between 20 and 80° (2θ) at a scan rate of 12.0 ° 2θ/min. The surface composition and morphology were measured by a Jeol JSM-6700F scanning electron microscopy (SEM) system. Transmission electron microscopy (TEM) was applied, using a Tecnai G2 S-Twin F20 TEM instrument. The thermal stability of FeNi/CS was investigated using a Netzsch STA 449C TGA Q500 analyzer under an air-flow with a heating rate of 10 ^{o}C/min from room temperature to 800 ^{o}C. The BET (Brunauer Emmett Teller) specific surface area was evaluated by N_2 adsorption method using an ASAP 2420 system (McKesson Corporation, USA). The static magnetic properties were investigated at 300 ^{o}C using a magnetic property measurement system (SQUID-VSM, Quantum Design). Fourier transform infrared spectra was obtained with Bruker IFS-66V/S FTIR spectrometer, which was recorded from 400–4000 cm^{-1}.

Application of FeNi/CS particles for the removal of TCE

TCE removal efficiency of FeNi/CS particles was compared with carbon spheres. The adsorption experiments were performed in 22 mL amber colored glass vials capped with Teflon Mininert valves. Aqueous TCE (204.4 mg/L) was added to the vials with 0.01 g of the material. The vials were filled with no headspace to minimize the volatile loss of TCE.[29, 39] Then it was placed on a horizontal shaker (300 rpm) at 25 ^{o}C. At a set time interval, 1 mL of solution was withdrawn by a syringe and filtered through a millipore film and the concentration of TCE was determined by high performance liquid chromatography (HPLC, Varian) with a UV detector set at λ = 214 nm. A C-18 column was employed to separate the organics. The mobile phase was a mixture of 85:15 (V:V) acetonitrile and water, with a flow rate of 1.0 mL/min. In recycled experiments, FeNi/CS can be separated easily from solution by applying a magnet, washed by water and ethanol and dried at 80 °C in air for next reuse.

The removal of TCE on FeNi/CS was calculated using the mass balance equation: $q_t = (c_o - c_t)\ v/m$, where q_t is the TCE concentration at time t in mg g^{-1}; v is the volume of TCE aqueous solution in L; m is the mass of the adsorbent in g; c_0 is

the TCE initial concentration, c_t is the TCE concentration at time t in mg g^{-1}.

The pseudo-first-order and pseudo-second-order (PSO) kinetics equation were used to investigate the adsorption mechanism of TCE on adsorbents (Table 1).[40-42] The pseudo-first-order (Equation a) and pseudo-second-order (Equation b) kinetics equations were expressed as follows:

$\ln (q_e - q_t) = \ln q_e - k_1' t$ (a)

$t/q_t = 1/k_2' q_e^2 + (1/q_e)t$ (b)

where q_e is the equilibrium TCE concentration in mg g^{-1}, and k_1' (min^{-1}) and k_2'(g mg^{-1} min^{-1}) are the rate constants of pseudo-first-order and pseudo-second-order kinetic models.

Table 1 Kinetic models and their mathematical expressions used to fit the data.

Model	Mathematical expression	Plot	Parameters
Pseudo-first order	$\ln(q_e-q_t)=\ln q_e - k_1' t$	$\ln(q_e-q_t)$ vs t	k_1'=slope q_e=intercept
Pseudo-second order	$t/q_t = 1/k_2' q_e^2 + (1/q_e)t$	t/q_t vs t	k_2'=slope^2/intercept q_e=1/slope

Results and discussions

Preparation of FeNi/CS

In the present work, metal ions M^{n+} (Fe^{3+} and Ni^{2+}) and OH^- ions together with glucose were dissolved to make a solution. After the mixed system was hydrothermally treated at 180 °C for 22 h, heterogeneous precursors of M(OH)x, and MO_x formed, as confirmed by XRD results in Fig. S1. FeNi alloy was produced by the self-reduction of these precursors that were immersed in the reductive environment resulted from the graphitization of hydrothermal carbon by calcination. The reaction process is briefly illustrated in Scheme 1.

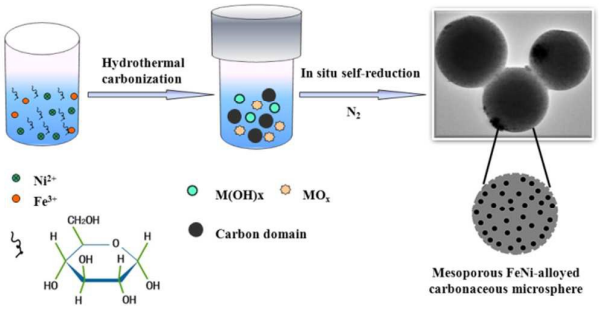

Scheme 1. Schematic illustration of the preparation process for FeNi/CS.

Characterization of FeNi/CS

Fig.1. exhibits X-ray diffraction (XRD) patterns of FeNi/CS. The peaks at 44.20°, 51.48°, 75.68° observed in all the three samples can be well ascribed to the (1 1 1), (2 0 0) and (2 2 0) faces of FeNi alloy (JCPDS NO. 65-3244, space group $Pm\bar{3}m$). Almost no other impurity phases like iron and nickel oxides or hydroxides are detected, suggesting the successful formation of pure phase crystalline FeNi alloy. The FeNi/CS-900 showed a sharp peak located at 25.36°, which belongs to the (0 0 2) face of graphitic carbon.[43] No peaks assigned to graphitic carbon were observed in the XRD patterns of FeNi/CS-500 and FeNi/CS-700, implying that the carbon component formed by the carbonization of glucose is mostly amorphous. This low crystallinity nature was then further subjected to the characterization by the Raman spectroscopy.[29,44,45]

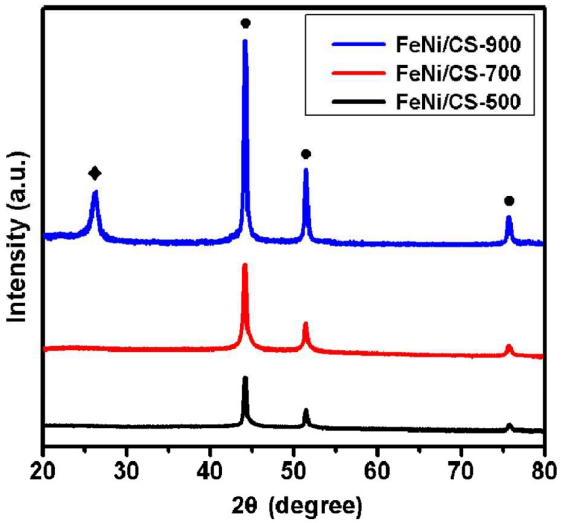

Fig. 1. XRD patterns of FeNi/CS-500, FeNi/CS-700 and FeNi/CS-900.

Raman spectroscopy was used to investigate the presence and crystallinity of carbon shells, as shown in Fig. 2. The three samples consist of two broad overlapping bands at around 1360 and 1587 cm^{-1}. The D band at 1360 cm^{-1} represents the disordered or low-symmetry carbon, and G band at 1587 cm^{-1} implies the presence of sp^2 hybrid graphitic carbon,[44] both indicating the existence of carbon component in the products. The appearance of an additional 2D band at 2698 cm^{-1} in the spectra of FeNi/CS-900 approves it to be a graphene sheets-contained carbon material, which is consistent with the higher ordered carbon structure expressed by its XRD pattern.[30] Based on all the data above, it is rational to conclude that the as-obtained products are magnetic composites composed of FeNi nanoparticles and carbon.

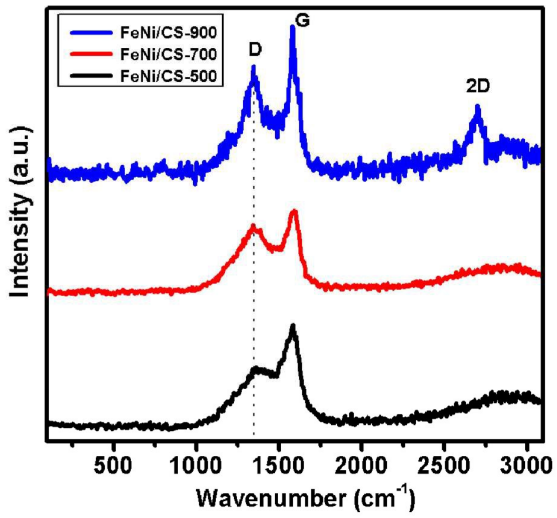

Fig. 2. Raman spectra of FeNi /CS samples.

Fig. 3. shows the thermo-gravimetric curves of FeNi/CS, which were used to determine the carbon content in those samples. The TGA data of FeNi/CS-500, FeNi/CS-700 and FeNi/CS-900 showed a total weight loss of about 77.52%, 76.93% and 71.89%, respectively. The gradual decreased carbon content implies the more consumption of carbon under higher calcination temperature, in which FeNi/CS-900 is found to possess the least carbon percentage. The residue phases of Fe_3O_4 and NiO as the final oxidation of interior metal were determined by XRD results in Fig. S2.[30,46-48]

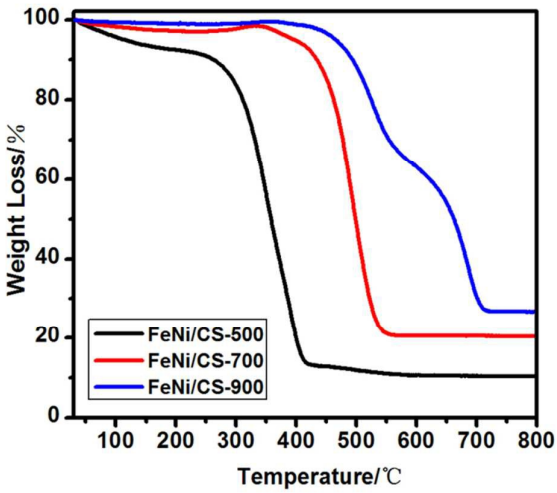

Fig. 3. TGA profiles of FeNi/CS in air atmosphere.

The morphologies of FeNi/CS samples are investigated by SEM (Fig. 4). It is obvious here that FeNi/CS-500 composite exhibits a typical micro-spherical morphology with smooth surface and size ranging from approximately 3-8 µm (Fig. 4a and 4d). Calcination temperature does not influence the spherical morphology, but the surface roughness is gradually changed for the samples of FeNi/CS-700 (Fig. 4b and 4e) and FeNi/CS-900 (Fig. 4c and 4f), as the pyrolysis temperature increases. Embedded FeNi alloy particles can be clearly visualized on the carbon surface of FeNi/CS-700 and FeNi/CS-900 upon the combustion of outermost carbon shell. This is also proved by the reducing carbon content from the TGA analysis. Their sponge-like structures confirm the existence of pores on the surface, which indicates the development of porous structure originating from the release of volatile substances during the hydrothermal carbonization of glucose under higher activation temperature.[49] This observation is consistent with the porosity analysis which will be further discussed in the nitrogen adsorption and desorption isotherms.

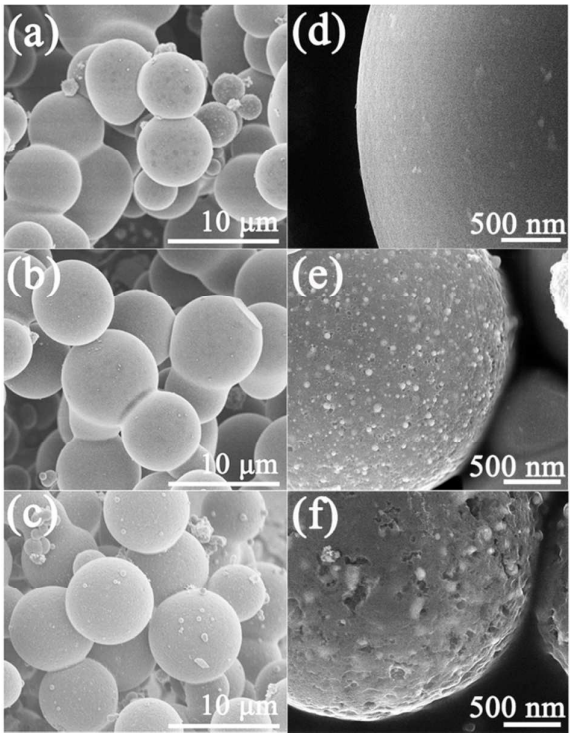

Fig. 4. Scanning electron microscopy (SEM) images of FeNi/CS-500 (a) and (d), FeNi/CS-700 (b) and (e), FeNi/CS-900 (c) and (f).

The microstructures of FeNi alloy/carbon sphere were further investigated by means of TEM. Fig. 5a shows the TEM image of FeNi/CS-700, presenting that the nanoscale FeNi alloy particles (dark dots) with average size around 10 nm are well dispersed and confined within the spherical carbon matrix (light sheath). This observation is quite consistent with the SEM image of Fig. 4e. The diameter of whole magnetic carbon spheres ranges from 3 to 5 µm, which is in accordance with the results from the SEM measurement. Fig. 5b exhibits the HRTEM image, which provides further insights into the structural information. The distance 0.208 nm and 0.179 nm are consistent with the (1 1 1) and (2 2 0) interplanar distances of FeNi alloy, which confirms the FeNi alloy composition of small black nanoparticles

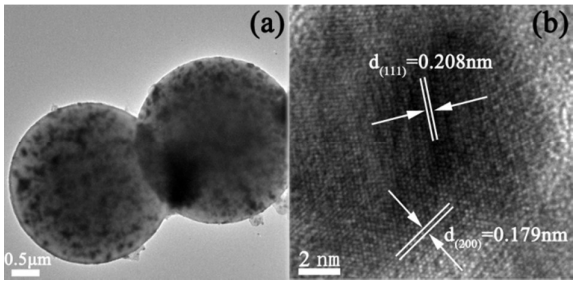

Fig. 5. Typical TEM image (a) and HRTEM micrograph (b) of FeNi/CS-700.

To investigate the pore structure characteristics of as-obtained magnetic carbon materials, which are critical factors in the application of adsorbents, N_2 adsorption/desorption isotherms are demonstrated in Fig. 6a, in comparison with carbon sphere. The representative type I isotherms of carbon sphere expresses its microporous nature. The combination of type IV (H_2 hysteresis loop at p/p_0 = 0.45-0.95, mesoporous structure) and type I (microporous structure) are found in the isotherms of FeNi/CS-700 and FeNi/CS-900, respectively.[50,51] However, none but the trivial micropores lie in the isotherms of FeNi/CS-500.

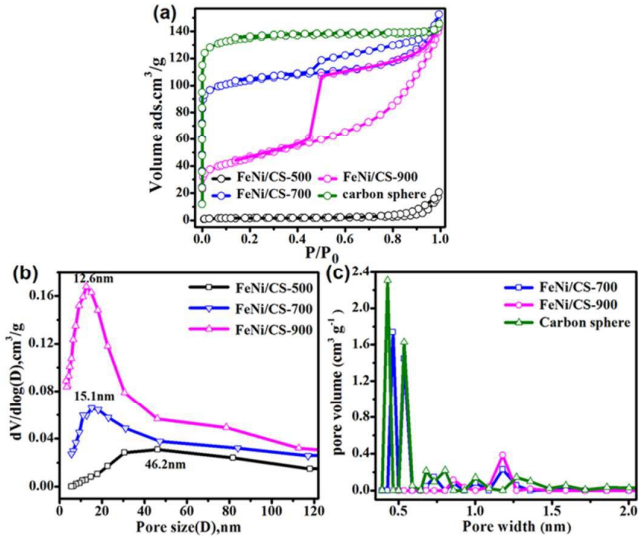

Fig. 6. (a) Nitrogen sorption isotherms. (b) mesopore size distributions (BJH method) and (c) micropore size distributions (NLDFT method) corresponding to FeNi/CS prepared at different carbonization temperatures.

In Table 2, carbon sphere obviously shows the highest BET specific surface area (441.01 m^2 g^{-1}). The surface area of magnetic carbon composites exhibits evident diminishment for FeNi/CS-500 (5.59 m^2 g^{-1}), FeNi/CS-700 (341.25 m^2 g^{-1}) and FeNi/CS-900 (157.59 m^2 g^{-1}). The variety of porosity can be resulted from the occupation of the effective surface area by FeNi alloy nanoparticles within the porous carbon matrix.[52] A fact can be deduced that the pyrolysis temperature has great influence on their porosity nature of the FeNi/CS samples. This could come from the formation of polymerized residue during glucose carbothermal process, which could hinder the continuity of pores and result in the least surface area at low temperatures (500 °C)[8]. At a higher temperature of 700 °C, the pores become accessible by the removal of volatile tar residue.[18] While the decreased porosity at 900 °C implies the consumption of more carbon component for the reduction of metal ions, consistent with the minimum carbon content based on TGA result.[18, 50] The suitable pyrolysis temperature makes FeNi/CS-700 to possess the most optimal porosity. A similar trend is found in their pore volume which follows the order of FeNi/CS-700 (0.236 cm^3 g^{-1}) > FeNi/CS-900 (0.221 cm^3 g^{-1}) > FeNi/CS-500 (0.032 cm^3 g^{-1}).

The pore size distributions corresponding to the mesopores and micropores of FeNi/CS are shown in Fig. 6b and 6c, respectively. It is particularly worth mentioning that FeNi/CS-700 and FeNi/CS-900 have two types of pores [51] which are deduced by the differential pore volume distribution vs. pore width plots using the NLDFT method in the case of the micropores (Fig. 6c) and the BJH method in the case of the mesopores (Fig. 6b).[10,53-55] The results are shown in Table 2. The pore size of FeNi/CS-500 is calculated to be around 46.2 nm which could mainly originate from the interparticle voids in virtue of the accumulation of particles, rather than internal pores. Sample of FeNi/CS-700 has a mesopore size centered at 15 nm and micropore size ranging from 0.46 nm to 1.18 nm. Increasing the temperature to 900 °C endows FeNi/CS-900 a mesopore centered 12 nm and micropore diameters of 0.85 nm and 1.18 nm. These results show clear evidence that pore size distributions of FeNi/CS were affected by temperature variation which plays a vital role on the adsorption capacity of TCE.

Table 2 Texture parameters deduced from nitrogen sorption isotherms on Carbon sphere and various FeNi/CS samples.

Property	Carbon sphere	FeNi/CS-500	FeNi/CS-700	FeNi/CS-900
BET surface area (m^2 g^{-1})	441.009	5.589	341.252	157.589
Langmuir surface area (m^2 g^{-1})	597.157	7.928	462.245	215.747
Total pore volume (cm^3 g^{-1})	0.225	0.032	0.236	0.220
Mesopore diameter (nm)	—	46.2	15.122	12.6211
Micropore diameter (nm)	0.43-1.59	—	0.46-1.18	0.86，1.18

Magnetic properties of FeNi/CS are investigated at room temperature. The hysteresis loops of the samples are shown in Fig.7 and the inset. All the samples exhibit typical ferromagnetic behavior.[29, 44] By calculating from VSM analysis, FeNi/CS-500, FeNi/CS-700 and FeNi/CS-900 display a hysteresis loop with saturation magnetization of 0.15 emu g^{-1}, 1.28 emu g^{-1} and 2.89 emu g^{-1}, respectively. The value of hysteresis (H_C) is about 16.5 Oe, 72.7 Oe and 146.2 Oe, respectively. FeNi/CS shows typically soft magnetic features, which make them magnetic field responsive, separated easily from the solution

with the help of an external magnetic force, and keep wonderful removal efficiency during five reusable cycles.

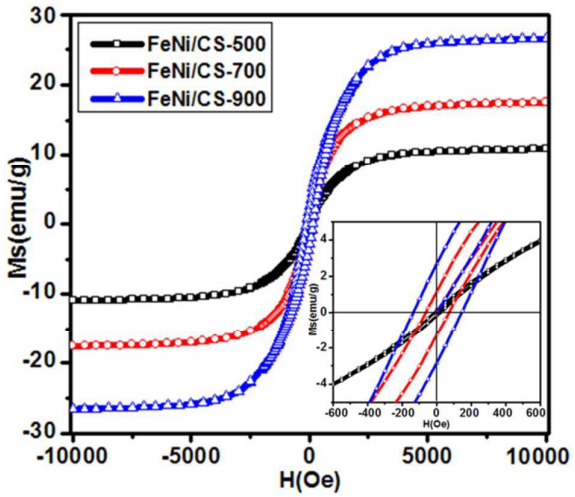

Fig. 7. Magnetization curves of FeNi/CS composites at room temperature and the inset shows the zoomed magnetization loops.

Adsorption behavior of the FeNi/CS composites

Batch adsorption capacity experiments were conducted to compare with FeNi/CS and carbon sphere in removing TCE from water. The plots in Fig. 8(a) presents the amounts of TCE adsorbed on various samples versus different contact times. The equilibriums were achieved completely within 240 min for all the samples. Rapid removal of TCE was obviously seen within 30-70 min, then it was followed by a slow adsorption progress in the remnant period to reach the maximum adsorption capacity. The two-phase adsorption can be explained by the abundant unoccupied sorption sites in samples, which are gradually saturated with time going by.[56] Maximum adsorption capacity of TCE by various samples was in the order of FeNi/CS-700>FeNi/CS-900>carbon sphere> FeNi/CS-500. The lowest removal ability of FeNi/CS-500 can be explained as its lack of effective pore structure compared to others, as discussed in the N_2 adsorption/desorption isotherms shown in Fig. 6. The adsorption capacity of TCE by carbon sphere, which has the highest surface area, is surprisingly lower than that of FeNi/CS-700 and FeNi/CS-900. As illustrated in the reported literature, the presence of micropores provides the interaction potential between adsorbent and adsorbate, whereas the mesopores induce the capillary condensation.[8] The sole presence of micropores in carbon sphere with small pore size between 0.43-1.59 nm may cause the deficient of adsorbent-adsorbate interaction which results in the poor TCE removal capacity. By comparing with their porosity characterization in Table 2, a facile entrance for TCE molecule are provided by the coexistence of compatible microporous and mesoporous structure in FeNi/CS-700 and FeNi/CS-900, thus making better adsorption performance.[18] Larger specific surface area of FeNi/CS-700, compared with FeNi/CS-900, leads to their difference in adsorption ability, even if they have a similar pore size. Therefore, the adsorption process is primarily related to pore size and surface area in the application of removing TCE contaminant.

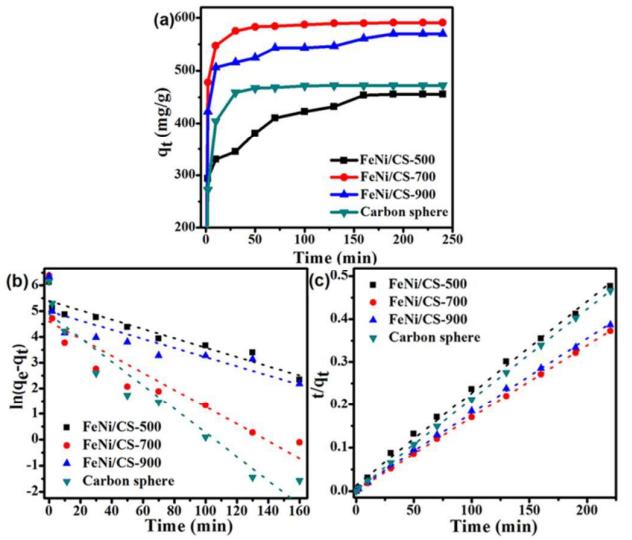

Fig. 8. TCE adsorption kinetics on different samples derived from FeNi/CS and Carbon sphere (Initial TCE concentration: 204.4 mg L^{-1}; adsorbent dose: 0.01 g) (a); Linear regression fittings of a pseudo-first order (b) and pseudo-second order (c).

The kinetic model parameters of these samples by linear regressions were shown in Table 3 and Fig. 8(b) and 8(c) The higher correlation coefficients (R^2) of pseudo second-order compared to that of pseudo-first-order suggests the adsorption of TCE onto the porous composites fits better for the pseudo-second-order (PSO) kinetic model, which can be assumed as heterogeneous chemisorption mechanism.[57] The active available adsorption sites as well as the van der waals forces between TCE molecules and carbon system of adsorbents facilitate the path, similarly illustrated in the adsorption mechanisms of Al_2O_3/MWCNTs.[58,59] The adsorption of TCE molecules by FeNi alloy encapsulated in carbon spheres can be further confirmed by FTIR spectra (Fig. S3).

Fig. 8c shows their perfect fits of the PSO model for the TCE adsorption kinetics data,[18,41,42] from which the adsorption capacity (q_e) and the rate constant (k_2') can be derived. The rate constant (k_2') determines the time required to reach an equilibrium-state. The k_2' values for different adsorbents range from 3.4×10^{-4} to 2.6×10^{-3} g mg^{-1} min^{-1} and follow the order of FeNi/CS-700>carbon sphere > FeNi/CS-900>FeNi/CS-500. The high k_2' values of FeNi/CS-700 and carbon sphere indicate the rapid mobility of TCE reaching the solid surfaces in a short time interval. The q_e values obtained from the kinetic model ranges from 462 to 590 mg g^{-1} for different adsorbents. It follows the order: FeNi/CS-700> FeNi/CS-900>carbon sphere > FeNi/CS-500. The high q_e values for FeNi/CS-700 (590.00 mg g^{-1}) and FeNi/CS-900 (569 mg g^{-1}) could be attributed to their high surface area imparted at high pyrolysis temperature and their compatible microporous and mesoporous structure.[18]

Table 3 Adsorption rate constants and correlation coefficients for pseudo-first-order and pseudo-second-order kinetic models.

Model	Parameter	FeNi/ CS-500	FeNi/ CS-700	FeNi/ CS-900	Carbon sphere
Pseudo-first-order	q_e (mg g^{-1})	5.4	4.6	4.99	4.89
	k_1 (min^{-1})	0.01811	0.3328	0.01776	0.04615
	R^2	0.89	0.82	0.7	0.917
Pseudo-second-order	q_e (mg g^{-1})	462	590	569	472
	k_2′(g mg^{-1} min^{-1})	3.4×10^{-4}	2.6×10^{-3}	7.16×10^{-4}	2.14×10^{-3}
	R^2	0.99	0.99	0.99	0.99

The reusability of FeNi/CS-700

The reusability of adsorbent is an important factor in evaluating practical environmental applications. The cycle test of adsorption capacity by FeNi/CS-700 was conducted by batch adsorption experiment of TCE. The magnetic carbon material was washed thoroughly after each cycle, with the mixture of ethanol and distilled water. Then it was separated by a magnet conveniently, dried at 80°C and used for next experiment. The regenerated FeNi/CS-700 showed a slightly declining performance in the second, third, fourth and fifth adsorption experiments compared to that of the freshly prepared particles (Fig. 9), in which the TCE removal efficiency dropped from 97 % to 75 % accordingly. The decrease in adsorption ability is presumably due to occupancy of active adsorption sites which determine the ability of FeNi/CS-700 to adsorb TCE. Therefore, the materials produced in our study are reusable and recyclable without sacrificing too much of its efficiency after the 5th time of regeneration.

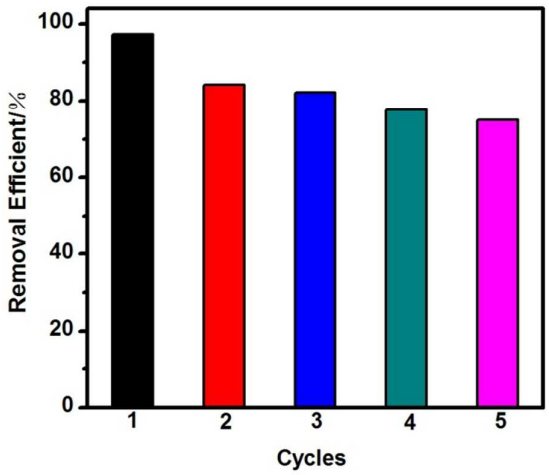

Fig. 9. The final removal efficiencies of TCE onto FeNi/CS-700 within 160 min during five adsorption-desorption cycles.

Conclusions

In summary, a facile one-pot carbonization reduction strategy for the synthesis of magnetic mesoporous FeNi/CS composites was demonstrated in this work. Microspherical morphology of FeNi/CS composites was determined with different porosity structures, which were related to the pyrolysis temperature. The as-prepared magnetic carbonaceous adsorbents showed excellent removal efficiency in the application of removing TCE contaminant and the adsorption process was well described by the pseudo-first-order model. FeNi/CS-700 has a highest adsorption capacity of 590.00 mg g^{-1} due to its high surface area imparted at high pyrolysis temperature and compatible microporous and mesoporous structure. Meanwhile, it retains good adsorption behavior after 5 adsorption-regeneration cycles via magnetic separation. This discovery offers a simple and effective way to obtain powerful magnetic carbon material which can be applied as a potential adsorbent for water purification.

Acknowledgements

This work was supported by grants from National Natural Science Foundation of China (No. 21401070 and 21201073), Natural Science Foundation of Jilin Province (No. 201215028), S&T Development Program of Jilin Province (No.20130522128JH, 20140520078JH, 20150204030GX).

References

1 Y. Min, G. He, Q. Xu, Y. Chen, J. Mater. Chem. A, 2014, **2**, 1294.
2 J. Su, Y. Zhang, S. Xu, S. Wang, H. Ding, S. Pan, G. Wang, G. Li, H. Zhao, Nanoscale, 2014, **6**, 5181.
3 V.S. Priya, L. Philip, *Chem. Eng. J.* 2015, **266**, 309.
4 D. Suma, D. Deng, *ACS Sustainable Chem Eng.* 2015, **3**, 133.

5 Z. Wei, Y. Seo, *J. Hazard. Mater.* 2010, **181**, 147.
6 B. Chang, D. Guan, Y. Tian, Z. Yang, X. Dong, J Hazard Mater, 2013, **262**, 256.
7 Z. Wang, C. Fang, M. Megharaj, *ACS Sustainable Chem Eng*, 2014, **2**, 1022.
8 M. Ahmad, S.S. Lee, A.U. Rajapaksha, M. Vithanage, M. Zhang, J.S. Cho, S.E. Lee, Y.S. Ok, Bioresour Technol, 2013, **143**, 615.
9 X. Sun, Y. Li, *Angew Chem*, 2004, **43**, 597.
10 Z. Yue, J. Economy, *J. Nanopart. Res.*, 2005, **7**, 477.
11 R.A. Brown, A.K. Kercher, T.H. Nguyen, D.C. Nagle, W.P. Ball, *Org Geochem.* 2006, **37**, 321.
12 M.M. Titirici, R.J. White, N. Brun, V.L. Budarin, D.S. Su, F. del Monte, J.H. Clark, M.J. MacLachlan, *Chem. Soc. Rev*, 2015, **44**, 250.
13 X. Zhu, Y. Liu, C. Zhou, G. Luo, S. Zhang, J. Chen, Carbon, 2014, **77**, 627.
14 A.M. Cooper, K.D. Hristovski, T. Moller, P. Westerhoff, P. Sylvester, J Hazard Mater, 2010, **183**, 381.
15 C. Liang, P.H. Lee, J Hazard Mater, 2012, **231**, 120.
16 S.-H. Hsu, C.-S. Huang, T.-W. Chung, S. Gao, *J. Taiwan. Inst. of Chem. E.* 2014, **45**, 2526.
17 H.H. Tseng, J.G. Su, C. Liang, J Hazard Mater, 2011, **192**, 500.
18 M. Ahmad, S.S. Lee, S.E. Oh, D. Mohan, D.H. Moon, Y.H. Lee, Y.S. Ok, *Environ. Sci. Pollut. R*, 2013, **20**, 8364.
19 R. Xiong, Y. Wang, X. Zhang, C. Lu, RSC Adv, 2014, **4**, 22632.
20 L.M. Rossi, N.J.S. Costa, F.P. Silva, R. Green Chem, 2014, **16**, 2906.
21 L. Yan, L. Kong, Z. Qu, L. Li, G. Shen, *ACS Sustainable Chem Eng*, 2015, **3**, 125.
22 Y.F. Su, Y.L. Cheng, Y.H. Shih, J Environ Manage, 2013, **129**, 361.
23 Z. Liu, F.-S. Zhang, *Bioresource Technol.* 2010, **101**, 2562.
24 H. Tang, D. Zhu, T. Li, H. Kong, W. Chen, *J.Environ. Qual*, 2011, **40**, 1878.
25 Y. Huang, A.A. Keller, *ACS Sustainable Chem Eng*, 2013, **7**, 731.
26 O.V. Kharissova, H.V.R. Dias, B.I. Kharisov, RSC Adv., 2015, **5**, 6695.
27 R. Ferrando, J. Jellinek, R.L. Johnston, *Chem Rev.* 2008, **108**, 845.
28 G. Abellán, E. Coronado, C. Martí-Gastaldo, A. Ribera, T.F. Otero, *Part Part Syst Char.* 2013, **30**(10), 853.
29 X. Lu, G. Huo, X. Liu, G. Liang, Z. Han, X. Song, CrystEngComm, 2012, **14**, 5622.
30 G. Abellán, J.G. Martínez, T.F. Otero, A. Ribera, E. Coronado, 2014, **39**, 15.
31 [31] Y. Wang, M. Yao, Y. Chen, Y. Zuo, X. Zhang, L. Cui, *J. Alloy. Compd*, 2015, **627**, 7.
32 Y. Tian, S. Zhong, A. Huang, Y. Pan, X. Wang, *Mater Lett.* 2015, **141**, 10.
33 R. Yang, Y. Wang, M. Li, Y. Hong, *ACS Sustainable Chem Eng*, 2014, **2**, 1270.
34 S. Zhang, N. Li, H. Lu, J. Zheng, R. Zang, J. Cao, RSC Adv., 2015, **5**, 50983.
35 H. Wang, Z. Chen, H.K. Liu, Z. Guo, RSC Adv, 2014, **4**, 65074.
36 D. Mohan, A. Sarswat, Y.S. Ok, C.U. Pittman, Jr., Bioresour Technol, 2014, **160**, 191.
37 S.R. Wild, S.J. Harrad, K.C. Jones, *Water Res.* 1993, **27**, 1527.
38 H. Li, Y. Dai, H. Huang, L. Li, S. Leng, J. Cheng, Y. Niu, H. Duan, Q. Liu, X. Zhang, X. Huang, J. Xie, Z. Feng, J. Wang, J. He, Y. Zheng, *Environ Health Persp.* 2007, **115**, 1553.
39 M. Ahmad, S.S. Lee, X. Dou, D. Mohan, J.K. Sung, J.E. Yang, Y.S. Ok, Bioresour Technol, 2012, **118**, 536.
40 X. Ma, X. Liu, D.P. Anderson, P.R. Chang, *Food Chem*, 2015, **181**, 133.
41 L.G. Yan, K. Yang, R.R. Shan, T. Yan, J. Wei, S.J. Yu, H.Q. Yu, B. Du, Kinetic, *J.Colloid Interf Sci*, 2015, **448**, 508.
42 H.H. Salih, C.L. Patterson, G.A. Sorial, R. Sinha, R. Krishnan, *Chem. Eng. J.* 2012, **193**, 422.
43 C.-H. Xu, L.-j. Zhu, X.-H. Wang, S. Lin, Y.-m. Chen, *Water Air Soil Poll.* 2014, **2**, 225.
44 S.J. Yan, C.Y. Xu, J.T. Jiang, D.B. Liu, Z.Y. Wang, J. Tang, L. Zhen, *J. Magn. Magn. Mater.* 2014, **349**, 159.
45 Y. Sun, X. Liu, C. Feng, J. Fan, Y. Lv, Y. Wang, C. Li, *J. Alloy Compd.* 2014, **586**, 688.
46 H. Qiao, Q. Luo, J. Fu, J. Li, D. Kumar, Y. Cai, F. Huang, Q. Wei, *J. Alloy Compd.* 2012, **513**, 220.
47 H. Sun, G. Zhou, S. Liu, H.M. Ang, M.O. Tade, S. Wang, *ACS Appl Mater Inter.* 2012, **4**, 6235.
48 S. Luo, F. Chai, T. Wang, L. Li, L. Zhang, C. Wang, Z. Su, RSC Adv, 2013, **3**, 12671.
49 H. Sun, G. Zhou, S. Liu, H.M. Ang, M.O. Tad, S. Wang, *ACS Appl Mater Inter.* 2012, **4**, 6235.
50 B. Qiu, Y. Wang, D. Sun, Q. Wang, X. Zhang, B.L. Weeks, R. O'Connor, X. Huang, S. Wei, Z. Guo, J. Mater. Chem. A, 2015, **3**, 9817.
51 A.B. Fuertes, M. Sevilla, *ACS Appl Mater Inter.* 2015, **7**, 4344.
52 J. Zhu, H. Gu, J. Guo, M. Chen, H. Wei, Z. Luo, H.A. Colorado, N. Yerra, D. Ding, T.C. Ho, N. Haldolaarachchige, J. Hopper, D.P. Young, Z. Guo, S. Wei, *J. Mater. Chem*, 2014, **2**, 2256.
53 K. Vaarmets, S. Sepp, J. Nerut, E. Härk, I. Tallo, E. Lust, *J Solid State Electr.* 2013, **17**, 1729.
54 J. Wang, S. Xu, Y. Wang, R. Cai, C. Lv, W. Qiao, D. Long, L. Ling, RSC Adv, 2014, **4**, 16224.
55 A. Silvestre-Albero, J. Silvestre-Albero, M. Martínez-Escandell, F. Rodríguez-Reinoso, *Ind Eng Chem Res.* 2014, **53** , 15398.
56 A. Saeed, M. Akhter, M. Iqbal, *Sep Purif Technol.* 2005, **45**, 25.
57 L.G. Yan, K. Yang, R.R. Shan, T. Yan, J. Wei, S.J. Yu, H.Q. Yu, B. Du, *J. Colloid. Interf . Sci.* 2015, **448**, 508.
58 S. Li, Y. Gong, Y. Yang, C. He, L. Hu, L. Zhu, L. Sun, D. Shu, *Chem Eng J.* 2015, **260**, 231.
59 J. Liang, J. Liu, X. Yuan, H. Dong, G. Zeng, H. Wu, H. Wang, J. Liu, S. Hua, S. Zhang, Z. Yu, X. He, Y. He, *Chem Eng J*, 2015, **273**, 101.